The role of roughness and porosity on the self-cleaning and anti-biofouling efficiency of TiO2-Cu and TiO2-Ag nanocoatings applied on fired bricks

# The role of roughness and porosity on the self-cleaning and anti-biofouling efficiency of $TiO_2$-Cu and $TiO_2$-Ag nanocoatings applied on fired bricks.

Lorenzo Graziani[a*], Enrico Quagliarini[a], Marco D'Orazio[a]

[a] *Department of Construction, Civil Engineering and Architecture (DICEA), Università Politecnica delle Marche, via Brecce Bianche, 60131, Ancona, Italy*

*e-mail: lorenzo_graziani@virgilio.it, e.quagliarini@univpm.it, m.dorazio@univpm.it*

**Keywords:** Porosity, Roughness, fired brick biodeterioration, Titania, Ag and Cu, nano-Coatings

## Abstract

From the advent of nanotechnologies in building constructions, many materials were functionalized to create composite material with new properties.
Titania ($TiO_2$) is actually the most promising nanotechnology to create composite materials with self-cleaning and anti-microbial properties. $TiO_2$ was able to limit algae adhesion and their growth, even if, in case of high porous and rough substrata, their inhibitory effect seems to be limited. This way, in this study, silver and copper nano-particulate enhanced an aqueous nano-titania solution were applied on brick specimens and their inhibitory effects were tested during accelerated laboratory tests.
Extent of biofouling on specimens' surface was assessed by measuring the aesthetical alteration and correlations between algal growth and key parameters of substrata were discussed.
Results confirm the key role of porosity and roughness on the biofouling process on untreated specimens, and their effect on the photocatalytic power of the tested nano-coatings toward algal adhesion.
Results from this study were compared with previous findings in the literature on the same types of specimens only treated with the same aqueous nano-titania solution. No significant improvements were detected by the addition of metal nanoparticles.
Experimental curves were overlapped to analytical model calculated by Avrami's law, and its validity was confirmed where latency time could be observed. Whereas no latency time was detected, that is a very fast adhesion of algal cells occurred, the experimental curves were modelled by using a four parametric logistic model that was able to describe numerically the biofouling process.

## 1. Introduction

The use of nanotechnologies in building construction was rapidly developed from its discovery [1], bringing to a new generation of functionalized building materials able to respond to new needs from the market.

In the fields of restoration of ancient buildings, and maintenance of new constructions, the use of titanium dioxide ($TiO_2$) finds large applications in components for self-cleaning and air pollution reduction [2–9].

An emerging application of this nanotechnology is the prevention of biodeterioration caused by microorganisms able to adhere on building's components where ideal conditions of light, temperature and moisture is present whereas this last one is a needful factor [10]. Green algae and cyanobacteria can be considered the most abundant colonisers of building façades, and microorganisms can produce aesthetical alterations like stains or colour variations depending on species.

The formation of biofilm helps to establish other vegetative species like lichens or bryophytes that increase water retention by substrata. Under these conditions, hydrodynamic of porous media changes [11], degradation mechanisms accelerate [12–14], and energy efficiency of the building could be reduced.

The use of nano-coatings is currently the new trend in biofouling prevention and many research papers can be found in the literature [15–31].

Recently, their application was studied for anti-biofouling scope on natural materials like stone [32–34], and man-made materials like brick [18,26,27,35], concrete [23,24,36] and mortar [17,25,28].

Literature shows anti-biofouling efficiency of nano-particles is strictly related to intrinsic characteristics of substrata, mainly porosity and roughness [10,35,37–41]. The influence of these parameters on inhibitory efficiency of $TiO_2$ was previously studied also on clay brick [26] and $TiO_2$ was unable to stop algal growth when it was applied on high porous material with rough surface, like clay brick applied in Cultural Heritage. In these conditions, porosity helps retention of water and nutrient for algal growth, while roughness favours the adhesion of algal cells to substrata and the inhibitory effect of $TiO_2$ is limited [26].

Some studies investigate the possibility of enhancing the photocatalytic power of $TiO_2$ by the addition of other metal nanoparticles, meanly silver (Ag) [42–44], and copper (Cu) [45].

A $TiO_2$-Ag solution was deposited on titania surface to test sanitation of *Escherichia coli*, and results show antibacterial properties also under visible light [42]. A sol–gel $TiO_2$-based coating with bioactive silver has been proposed as a promising strategy for controlling in vitro biofilm formation of *Escherichia coli* and

59 *Staphylococcus epidermidis* [43]. Results of this study showed that AgCl–$TiO_2$ nano-composite coated
60 surfaces inhibited the development of biofilm over a period of 10 days in accelerated conditions.
61 These two studies were carried out on neutral substrata, and it is not possible to find the effect of substrata
62 (i.e. building materials) on the biocide power of nano-coating.
63 Silver nano-particulate enhanced aqueous silane/siloxane emulsion was applied on mortar surface, and a
64 significant reduction of biofouling surface coverage and its intensity were observed [44]. The author
65 provides also information about silver concentration, indeed a concentration above 0.5% (wt) could cause
66 aesthetical alteration, and water contact angle improvement was negligible against increased material cost
67 [44]. Thus, a synergism between antimicrobial properties and photo-disinfection properties of $TiO_2$ was
68 observed in the literature.
69 In this study, two nanostructured solutions of $TiO_2$-Ag and $TiO_2$-Cu were respectively applied on two
70 different clay brick substrata to investigate their inhibitory efficiency toward algae and cyanobacteria.
71

72 ## 2. Material and methods

73 ### *2.1. Material preparation and characterization*

74 In order to consider the effect of substrata, two types of specimens were prepared with different total
75 porosity and roughness.
76 High porous specimens (group A) were moulded in rectangular moulders and left at ambient conditions until
77 the dry weight was reached. Specimens were then removed from the moulds and fired at about 700°C. This
78 production method was used because it replicates traditional clay brick production methods used in Cultural
79 Heritage.
80 Low porous specimens (group N) were produced by modern technique. After mixing, they were extruded
81 and then fired at about 1200°C. This production process is currently used to produce fired clay elements for
82 application in building façades and ventilated building façades.
83 Eighteen specimens were prepared for each group with final dimensions equal to 80x80x30 $mm^3$.
84 Surface roughness parameters were evaluated according to European standards [46,47] by using a Diavite
85 DH-5 portable rugosimeter. Arithmetic average (*Ra*), maximum profile peak height (*Rz*) and maximum
86 height of the profile (*Rmax*) were calculated according to UNI EN ISO 4287:2009 [47]. Each parameter was

87 obtained by ten measurements on a track of 15mm with a cut-off length of 0.8mm. The first and last values
88 were excluded to limit measurement's noise. Thus, the active track of measurement was equal to 13.4mm.
89 Porous structure (total porosity and porous distribution) were measured onto five N and five A additional
90 samples by a mercury intrusion porosimeter (Micromeritics Autopore III) following the ASTM D4404–10
91 standard [48].
92
93 *2.2. Nano-coating application*
94 Two types of aqueous $TiO_2$-based solutions were studied in this paper. The first $TiO_2$ solution was doped
95 with silver nanoparticles, while the other one was doped with copper nanoparticles. $TiO_2$-Ag nano-powders
96 were composed by $TiO_2$ and a concentration of silver and copper nanoparticles equal to 1% (molar
97 weight/$TiO_2$ weight). Concentration of $TiO_2$-Cu solution was equal to 1% (weight/$TiO_2$ weight). Final
98 concentration of aqueous solutions was equal to 1% (weight/volume of water). Thus, 100ml of solution
99 contains 1g of $TiO_2$ and 0.02g of Ag and 0.01g of Cu, respectively.
100 These concentrations were chosen to avoid browning of nano-film during UV irradiation, as demonstrated by
101 preliminary tests (not reported in this paper). This phenomenon was also previously shown in the literature
102 with a concentration of Ag equal to 1.48mol% to titania [42].
103 Both aqueous solutions were manually applied on the specimens' surface by spray coating. An air spray gun
104 with a nozzle of 0.8 mm diameter was connected to an air compressor at a pressure of 7 bar and was used to
105 spray the solutions from a distance of 250 mm. Specimens were then dried at 60°C for 1 h to accelerate the
106 drying process.
107 For each group (A and N), three specimens were treated with $TiO_2$-Ag (AAg and NAg) and $TiO_2$-Cu (ACu
108 and NCu) respectively, whereas three specimens remained untreated (ANt and NNt) to be used as references.
109 Colour measurements were made in accordance to UNI-EN 15886 [49] with a portable spectrophotometer
110 (Konica Minolta CM 2600d).
111 Colour variation between original specimens and treated ones was calculated following equation 1:

$$\Delta E = \sqrt{(L_0^* - L^*)^2 + (a_0^* - a^*)^2 + (b_0^* - b^*)^2} \quad 1)$$

112

where $L^*_0$, $a^*_0$ and $b^*_0$, and L*, a* and b* are colour coordinates of original specimens and treated ones respectively.

### 2.3. Photocatalytic efficiency of nano-coatings

Self-cleaning ability of $TiO_2$ nano-coating was evaluated by considering the degradation of organic dye (Methylene Blue – MB) following the same methods proposed in the literature [50].

Briefly, 0.5ml of MB aqueous solution (MB content: 100 μmol/L) was deposited on an area of 2200 $mm^2$ on the surface of brick specimens (80x80x30 $mm^3$) by using a syringe, while one specimen for each type remained untreated, and it was considered as control.

UV irradiation was provided by an 8W Blacklight Blue neon (working at 365nm) at a distance of about 15 cm from the specimens' surface. In this way, UV irradiance value was equal to about 10 $W/m^2$.

Colour values were detected before UV irradiation and after 1, 2, 4 and 26 hours as specified by standard [51]. The discoloration efficiency ($R_E$) was measured during time by equation 2, and it was expressed as percentage.

$$R_E(\%) = \frac{\left|\Delta E_t^* - \Delta E_0^*\right|}{\Delta E_0^*} \times 100 \qquad 2)$$

$\Delta E_t^*$ in equation 2 is the average colour variation between the measured colour after 1, 2, 4 and 26 hours and the original surface colour before MB application, and $\Delta E_0^*$ is the average colour variation between the measured colour after MB application and the original surface colour.

### 2.4. Accelerated growth test and biofouling evaluation

Biofouling process was simulated into 100x40x53 $cm^3$ glass chamber whose architecture has been previously described [26,27,35]. Scheme of apparatus is illustrated in Fig. 1.

Broth culture was composed by *Chlorella cf. mirabilis* and *Chroococcidiopsis fissurarum*. The initial concentration of composed microbial suspension was about 4mg of algal cells in one litre.

137 Temperature and relative humidity (RH) inside the glass chamber were recorded every 5 min over the entire
138 period of accelerated test by using a remote data logger (Lascar Electronics model EL-USB-2). Plot in Fig. 2
139 shows climatic conditions inside the chamber near the specimens' position.
140 In order to furnish necessary light for photosynthesis of algal cells, two neon lamps with a light temperature
141 of 5000 K were inserted in the chamber, while UV radiation for $TiO_2$ activation was provided by one
142 Blacklight Blue neon at a distance of about 150mm from the specimens' surface. In this way, nanocoating
143 was irradiated with an average UV intensity of 8 $W/m^2$. The day/night period was equal to 14/10 hours
144 respectively.
145 Above the samples, a 10 mm diameter PVC rail containing three 2 mm holes for each specimen, was
146 attached to the rack. The distance from the rails to the sample surface was approximately 30 mm and
147 designed to allow water to fall approximately 10 mm from the top of the sample.
148 The chamber contained one 500 L/h water pumps attached to both rails using T-connectors. The run/off
149 cycle of water was 15 min for a duration of 6 h (3 h run and 3 h off).
150 Biofilm causes stain on the substratum both by the presence of extracellular polysaccharides (EPS) on the
151 surface of biofilm [52], and by the presence of organic colored pigments like chlorophyll a and b
152 (responsible of green colour) or carotenoids (responsible of orange colour).
153 For this reason, the colour of each specimens was also measured during the accelerated growth test following
154 the same procedure described in section 2.2.
155 In order to collect data about the extension of algal fouling, the surface of each specimen was periodically
156 (weekly) digitized by an office scanner. The adopted resolution was 600dpi because it was able to show the
157 comparison of algal spot (equal to one pixel) with a side of about 40μm. Obtained images were filtered and
158 binarized to isolate pixels occupied by algae, then colonized area was counted by ImageJ software, and
159 percentage of coverage was calculated from the total area of each specimen equal to 80x80 $mm^2$.

160 *2.5. Numerical modelling of biofouling*

161 In this paper, experimental results were overlapped to analytical curves calculated by the Avrami's law (3)
162 that shown to be adequate in the literature [53,54], especially in case of biofouling process with sigmoidal
163 trend.

$$X(t) = 1 - e^{-K(t-t_1)^n} \quad 3)$$

where $t_1$ is the latency time (corresponding to the comparison of the first algal spot), $K$ is a constant of the material, and $n$ is the Avrami's exponent calculated as indicated in equation 4.

$$n = q + 3 \quad 4)$$

The q parameter was derived from general equation of the growth that was linear in time, thus q can be assumed equal to one and n=4 consequently.

The K parameter includes other parameters dependent on the material properties, and it can be calculated from equation 5.

$$K = A\, k_g\, k_c^{\,2} \quad 5)$$

where kg is the rate of the nucleation of new particles, kc is the specific growth rate constant, and A is a constant calculated by equation 6.

$$A = \frac{2}{(q+1)(q+2)(q+3)} \quad 6)$$

In case of specimens covered by algae partially (covered area < 100%), equation 7 was used instead of equation 3 as previously proposed in the literature [54].

$$X(t) = (1 - e^{-K(t-t_1)^n}) \times S_{max} \quad 7)$$

## 3. Results and discussion

### *3.1. Properties of substrata*

Table 1 shows results about porosity and roughness of tested specimens. The differences between the two different substrata are evident. Specimens of group A were characterized by a total porosity of about 37%, twice than total porosity of specimens of group N. Moreover, average pore diameter of A specimens was about 0.4μm, while porosity of group N was composed by average pore diameter of about 0.1μm. Thus, specimens of group A had high porosity composed by low pores with large diameter, while group N was characterized by many pores with small diameter. This finding was confirmed by values of total pore area, indeed total pore area of group A was about three times of group N.

184 This last result was important because total pore area controls movements of water at the interface between
185 material and microorganisms as previously demonstrated [26,35].
186 Manufacturing methods also influenced morphology of the surface, particularly the roughness. The average
187 roughness of A specimens was about three times Ra of group N, while other roughness's parameters (*Rz* and
188 *Rmax*) were about twice in case of A specimens if compared with specimens of group N (Table 1).

189

190 ### *3.2. Colour variation after treatment*

191 The application of the coatings caused colour variations as indicated in Table 2. $TiO_2$-Ag sol caused a
192 difference in lightness in both A and N specimens; in case of A specimens, $\Delta L^*$ was twice than N specimens.
193 The same trend was notable in case of specimens treated with $TiO_2$-Cu solution. By looking at $a^*$ and $b^*$
194 coordinates, a higher variation of colour coordinates was visible in N specimens.
195 Thus, after coating applications, clay bricks showed whitening (higher $L^*$), and they become less red and
196 more yellow (lower $a^*$ and $b^*$). Total colour variation ($\Delta E$) was about the same in all specimens. $\Delta E$ was
197 greater than the just noticeable difference (JND) by naked eye fixed to 2.3 [55], and it was also a bit greater
198 than the value accepted for preservative treatments of historical building surfaces fixed to 5 [56].
199 Colour variation of specimens' surfaces was about the same observed on specimens treated with only $TiO_2$
200 solution [50], as expected.

201

202

203 ### *3.3. Self-cleaning ability of nano-coatings*

204 Fig. 3 shows the self-cleaning efficiency $R_E$ of tested specimens. Group A shows no efficiency of
205 nanocoatings, indeed AAg and ACu have the same trend of untreated ANt specimens. At the end of the test
206 the curves can be considered overlapped. Conversely, N specimens show a different trend. In this last case
207 untreated specimens reached an efficiency of about 9%, while $R_E$ of NAg was about 33% and it reached
208 about 46% in case of NCu specimens. Thus, $TiO_2$-based solutions shown a noticeable (three time higher)
209 self-cleaning ability in case of low porous specimens. Inefficiency of treatments in case of A specimens can

be ascribable to high porosity and roughness of substrata of course [10,35,37–40]. Secondly, it can be associated to micro-cracks on the surface of treatment that limits the photocatalytic efficiency of nano-coating [50].

### *3.4. Biofouling evaluation and discussion*

By considering the colour variation, no significant different exists between untreated A specimens and treated ones (Fig. 4 a). In case of low porous specimens N (Fig. 4 b), ΔE of untreated specimens was about twice than ΔE of treated ones at the end of the accelerated test.

No significant differences were notable between specimens treated with $TiO_2$-Ag sol and $TiO_2$-Cu sol in both A and N specimens. Anyhow, $TiO_2$-Ag specimens showed minor colour variation than $TiO_2$-Cu specimens. Colour change was related to phototropic activity of algal biofilm, and it was capable to detect the presence of algal cells, but it was not adequate to describe the extension of algal adhered to substrate. Thus, this technique was coupled to digital image analysis to measure the percentage of algal coverage as described in section 2.4 (Fig. 5).

Fig. 5 shows algal coverage during time of the accelerated growth test.

Investigating the anti-biofouling effect of nano-coatings, it is possible to conclude that $TiO_2$-Ag was able to inhibit algal growth better than $TiO_2$-Cu treatment, especially in case of A specimens

Algal coverage of $TiO_2$-Ag specimens was always lower than $TiO_2$-Cu specimens, in both A and N specimens (Fig. 5).

The effect of the coatings was better visible in case of N specimens, indeed the maximum coverage of treated samples was about 8%, while untreated samples reached about 22% (about three times higher).

A decrease of algal coverage was visible in Fig. 5 b after ten weeks on both control specimens and treated ones. The decrease was also visible on A specimens (Fig. 5 a) after eight weeks. These decreases were ascribable to natural dispersal phase of biofilm that enables biofilm to spread and colonize new surfaces. This phase starts after biofilm growth and maturation, when fluid is able to employ adequate forces (in relation to biofilm's thickness) [57]. Since biofouling process on A specimens was faster than on N specimens, the detachment phase occurred two weeks before.

These findings are in line with results from self-cleaning test (Section 3.3), indeed the higher is $R_E$, the higher is the ability to stop algal growth on specimens and vice versa.

By comparing the results from this study with previous finding on the same specimens only treated with $TiO_2$ sol [26], it is possible to highlight the effect of Ag and Cu addition.

243 High porous specimens with rough surface treated with $TiO_2$ sol reached 95.45±1.36% of algal coverage
244 [26], while $TiO_2$-Ag and $TiO_2$-Cu reached 94.88±3.24% and 96.43±0.95% respectively. Thus, no significant
245 differences were notable comparing the results, and the addition of Ag and Cu to $TiO_2$ sol (in the percentage
246 used in this study, that is, so as to not altering the aesthetic appearance too much) does not produce the
247 expected increment of biocide power.
248 Low porous specimens with less rough surface were covered by 3.64±0.50% if treated by only $TiO_2$, while
249 they reached 6.66±1.50% with $TiO_2$-Ag, and 8.24±2.74% with $TiO_2$-Cu.
250 In this last case, it seems that Cu and Ag promote algal growth on specimens' surface, but this phenomenon
251 could be caused by other factors (morphology of nano-coating, nano-particles deposition, etc…), and further
252 investigations are required before giving a conclusion.
253 Results from this study are in contrast with other finding in the literature [42–44], underling how the
254 efficiency of any coating cannot be assessed without testing them directly on each substratum they could be
255 applied. In fact, the previous contrast is mainly ascribable to different substrata (in vitro assay [42,43], and
256 mortar samples [44]) that play a key role in the biocide activity of titania [26].
257 The effects of intrinsic characteristics of substrata (porosity and roughness) is visible at a glance in Fig. 5.
258 The A specimens (with higher porosity and roughness) reached total coverage around at the fifth week of test
259 (Fig. 5 a), while N specimens (with low porosity and roughness) reached maximum 20% of algal coverage at
260 around the tenth week (Fig. 5 b). This phenomenon was foreseeable, indeed the influence of porosity and
261 roughness on clay brick was previously studied in the literature [26,35].
262 Porosity and roughness play a synergetic effect: the first contributes to retain water and nutrient into the
263 substrata, while the second offers asperities required for adhesion of algal cells,
264 Not only trend of algal coverage was confirmed, but also values of maximum algal extension was
265 substantially the same of previous researches [26].
266
267 *3.5. Modelling of biofouling process*
268 Fig. 6 shows the analytical curve, obtained by the Avrami's law, overlapped to experimental data. In case of
269 N specimens, the Avrami's law was used to modelize the biofouling process, and it was adequate to describe
270 the biofouling processes.

271 In case of specimens of group A, Avrami's law was very aloof from the experimental data. This result is
272 explicable by observing the shape of the biofouling process. In fact, no latency time was observed during the
273 experimental phase. The high porosity and roughness of the specimens caused a very fast adhesion of algal
274 cells, and biofouling process started immediately.
275 The existence of a latency time ($t_l$ exponent in equation 3), an exponential growth, and a stationary phase are
276 at the basis for the application of the Avrami's law, and they were not observed on specimens of group A
277 (Fig. 6 b).
278 Then, a different approach was followed and a four parametric logistic model (4PL) was used to describe
279 numerically the biofouling of group A (equation 8).

$$y = A + \frac{B - A}{1 + \left(\frac{C}{x}\right)^{D}} \qquad 8)$$

280 In the 4PL model, *A* is the minimum *y*, *B* is the top of the plateau of the curve (highest *y*), *C* represents the *x*
281 at the inflection point of the S-shaped curve, and *D* is the slope factor. Under these hypotheses, *A* was fixed
282 to zero, *B* was the maximum value of algal coverage varying from sample to sample, and *C* was equal to
283 seven (days) because the curve changed its curvature after the first week due to the very fast biofouling
284 growth (Fig. 5 a). The slope factor *D* was calculated by minimizing the standard deviation between
285 experimental and analytical curves. Results obtained by this operation are reported in Fig. 7.
286 The parameters obtained by the two models were resumed in Table 3 and Table 4.
287 In case of Table 3, the most indicative parameter to describe the biofouling process is $K_c$ that represents the
288 speed of the growth of algal spot. NNt shows higher $K_c$ (both experimental and calculated) than NAg and
289 NCu specimens. This means that nano-coating influenced the biofouling process, and slowed down its
290 expansion. In this way, biofouling on NAg and NCu specimens was less extended than biofouling on NNt
291 specimens (see Fig. 5 b and Fig. 6 a). In addition, Table 3 allows to compare the results of this research with
292 results of a previous research with only $TiO_2$ treatment on the same type of specimens [54], and it permits to
293 extend the range of Avrami's parameter in case of clay brick specimens.
294 Table 4 shows no significant difference between untreated samples and treated ones, indeed values indicate
295 the same trend. A little difference is visible in case of slope of the curves (D). In this case, AAg and ACu

296 show smaller D than ANt specimens. This means that the biofouling process was lightly slowed down by the
297 treatment, but the nanocoating was not able to stop the growth of algal cells that cover the specimens'
298 surfaces almost completely.
299
300 **4. Conclusions**
301 Previous researches on innovative treatments for biofouling prevention on brick substrata by the use of $TiO_2$
302 nanocoatings have shown how these are able to limit algae adhesion and their growth, even if, in case of high
303 porous and rough substrata, their inhibitory effect seems to be limited. This way, this paper investigates on
304 how the addition of Ag and Cu could fill in this gap.
305 Two types of brick were tested in order to simulate both ancient and contemporary brick façades.
306 Accelerated algal growth test was then carried out to study the effect of the addition of these nano-metals to
307 $TiO_2$ sol. Test was conducted in the same way of previous researches, and specimens with the same
308 characteristics were tested.
309 This study confirms the key role of porosity and roughness on the biofouling process, and on the biocide
310 effect of the tested nano-coatings. Besides, it underlines how the efficiency of any coating cannot be assessed
311 without testing them directly on each substratum they could be applied.
312 Anyway, the addition of silver and copper nano-particles to $TiO_2$ sol does not produce the expected effect on
313 like-ancient brick surface, while a certain decrement of algal adhesion was observed in modern brick
314 substrata. On the contrary, the results encourage the application of $TiO_2$ based nano-coatings for the
315 production of new composite material and components to prevent algal adhesion on modern building façades
316 and reduce the maintenance costs consequently.
317 Finally, in this paper, the validity of Avrami's law was confirmed to be adequate to predict the biofouling
318 processes that were described by a sigmoidal curve composed by an initial latency time, an exponential
319 growth, and a stagnation phase. In cases in which these three phases are not present, the hypotheses at the
320 base of Avrami's law are not no longer valid, and four parametric logistic model was proposed to modelize
321 the biofouling process. Analytical models (both Avrami's model and 4PL model) confirmed findings from
322 experimental data, and they could have the potentiality to predict biofouling process of algae on brick
323 specimens.

Further researches are currently under way to optimize the photocatalytic power of nano-coatings toward biofilm formation.

**Acknowledgments**

The authors wish to thank Salentec S.r.l. for the supply of nanostructured TiO2 titanium dioxide solutions. The authors wish also thank the Algotheque du Laboratoire de Cryptogamie of the MuseumNational d'Histoire Naturelle (MNHN) for the supply of algal cultures.

# References


[1] A. Fujishima, T.N. Rao, D.A. Tryk, Titanium dioxide photocatalysis, J. Photochem. Photobiol. C Photochem. Rev. 1 (2000) 1–21.

[2] M. Rastogi, R. Vaish, Visible light induced water detoxification through Portland cement composites reinforced with photocatalytic filler : A leap away from TiO 2, Constr. Build. Mater. 120 (2016) 364–372. doi:10.1016/j.conbuildmat.2016.05.114.

[3] D. Wang, Z. Leng, M. H??ben, M. Oeser, B. Steinauer, Photocatalytic pavements with epoxy-bonded TiO2-containing spreading material, Constr. Build. Mater. 107 (2016) 44–51. doi:10.1016/j.conbuildmat.2015.12.164.

[4] Q. Li, Q. Liu, B. Peng, L. Chai, H. Liu, Self-cleaning performance of TiO2-coating cement materials prepared based on solidification/stabilization of electrolytic manganese residue, Constr. Build. Mater. 106 (2016) 236–242. doi:10.1016/j.conbuildmat.2015.12.088.

[5] S. Bogutyn, C. Arboleda, A. Bordelon, P. Tikalsky, Rejuvenation techniques for mortar containing photocatalytic TiO<inf>2</inf> material, Constr. Build. Mater. 96 (2015) 96–101. doi:10.1016/j.conbuildmat.2015.07.192.

[6] M. V. Diamanti, B. Del Curto, M. Ormellese, M.P. Pedeferri, Photocatalytic and self-cleaning activity of colored mortars containing TiO2, Constr. Build. Mater. 46 (2013) 167–174. doi:10.1016/j.conbuildmat.2013.04.038.

[7] P. Krishnan, M.H. Zhang, Y. Cheng, D.T. Riang, L.E. Yu, Photocatalytic degradation of SO2 using TiO2- containing silicate as a building coating material, Constr. Build. Mater. 43 (2013) 197–202. doi:10.1016/j.conbuildmat.2013.02.012.

[8] P. Krishnan, M.-H. Zhang, L. Yu, H. Feng, Photocatalytic degradation of particulate pollutants and self-cleaning performance of TiO2-containing silicate coating and mortar, Constr. Build. Mater. 44 (2013) 309–316. doi:10.1016/j.conbuildmat.2013.03.009.

[9] E. Quagliarini, F. Bondioli, G.B. Goffredo, C. Cordoni, P. Munafò, Self-cleaning and de-polluting stone surfaces: TiO2 nanoparticles for limestone, Constr. Build. Mater. 37 (2012) 51–57. http://www.sciencedirect.com/science/article/pii/S0950061812004758.

[10] H. Barberousse, B. Ruot, C. Yéprémian, G. Boulon, An assessment of façade coatings against colonisation by aerial algae and cyanobacteria, Build. Environ. 42 (2007) 2555–2561. http://www.sciencedirect.com/science/article/pii/S0360132306002046.

[11] A.B. Cunningham, W.G. Characklls, F. Abedeen, D. Crawford, Influence of Biofilm Accumulation on Porous Media Hydrodynamics, Environ. Sci. Technol. 25 (1991) 1305–1311.

[12] N. Djongyang, R. Tchinda, D. Njomo, A study of coupled heat and mass transfer across a porous building component in intertropical conditions, Energy Build. 41 (2009) 461–469. http://linkinghub.elsevier.com/retrieve/pii/S0378778808002478 (accessed June 10, 2015).

[13] J. MacMullen, Z. Zhang, E. Rirsch, H.N. Dhakal, N. Bennett, Brick and mortar treatment by cream emulsion for improved water repellence and thermal insulation, Energy Build. 43 (2011) 1560–1565. http://linkinghub.elsevier.com/retrieve/pii/S0378778811000582 (accessed June 10, 2015).

[14] E. Rirsch, J. MacMullen, Z. Zhang, Evaluation of mortar samples obtained from UK houses treated for rising damp, Constr. Build. Mater. 25 (2011) 2845–2850. http://linkinghub.elsevier.com/retrieve/pii/S0950061810007415 (accessed June 10, 2015).

[15] F. Chen, X. Yang, H.K.C. Mak, D.W.T. Chan, Photocatalytic oxidation for antimicrobial control in built environment: A brief literature overview, Build. Environ. 45 (2010) 1747–1754. http://www.sciencedirect.com/science/article/pii/S0360132310000363.

[16] W. De Muynck, A. Maury-Ramirez, N. De Belie, W. Verstraete, Evaluation of strategies to prevent algal fouling on white architectural and cellular concrete, Int. Biodeterior. Biodegradation. 63 (2009) 679–689.

[17] A.J. Fonseca, F. Pina, M.F. Macedo, N. Leal, A. Romanowska-Deskins, L. Laiz, A. Gómez-Bolea, C. Saiz-Jimenez, Anatase as an alternative application for preventing biodeterioration of mortars: Evaluation and comparison with other biocides, Int. Biodeterior. Biodegradation. 64 (2010) 388–396.

[18] F. Gladis, A. Eggert, U. Karsten, R. Schumann, Prevention of biofilm growth on man-made surfaces: evaluation of antialgal activity of two biocides and photocatalytic nanoparticles., Biofouling. 26 (2010) 89–101. http://www.ncbi.nlm.nih.gov/pubmed/20390559 (accessed March 7, 2014).

[19] F. Gladis, R. Schumann, Influence of material properties and photocatalysis on phototrophic growth in multi-year roof weathering, Int. Biodeterior. Biodegradation. 65 (2011) 36–44.

[20] K. Gröplová, K. Čabanová, P. Bábková, M. Vaculík, V. Matějka, J. Kukutschová, P. Čapková, Testing the effects biodeteriorations green algae Chlorella Vulgaris on samples added photoactive composites kaoline/TiO2, in: 2nd Int. Conf. NANOCON, Olomouc, Czech Republic, 2010: pp. 1–6. http://www.nanocon.cz/files/proceedings/nanocon_10/lists/papers/403.pdf.

[21] N.B. Hartmann, F. Von der Kammer, T. Hofmann, M. Baalousha, S. Ottofuelling, A. Baun, Algal testing of titanium dioxide

nanoparticles--testing considerations, inhibitory effects and modification of cadmium bioavailability, Toxicology. 269 (2010) 190–197. http://www.ncbi.nlm.nih.gov/pubmed/19686796.

[22] J. Hong, H. Ma, M. Otaki, Controlling algal growth in photo-dependent decolorant sludge by photocatalysis, J. Biosci. Bioeng. 99 (2005) 592–597. http://www.ncbi.nlm.nih.gov/pubmed/16233836.

[23] C.A. Linkous, G.J. Carter, D.B. Locuson, A.J. Ouellette, D.K. Slattery, L.A. Smitha, Photocatalytic Inhibition of Algae Growth Using TiO2, WO3, and Cocatalyst Modifications, Environ. Sci. Technol. 34 (2000) 4754–4758. http://dx.doi.org/10.1021/es001080+.

[24] A. Maury-Ramirez, W. De Muynck, R. Stevens, K. Demeestere, N. De Belie, Titanium dioxide based strategies to prevent algal fouling on cementitious materials, Cem. Concr. Compos. 36 (2013) 93–100. http://www.sciencedirect.com/science/article/pii/S0958946512002053?v=s5.

[25] Z. Zhang, J. MacMullen, H.N. Dhakal, J. Radulovic, C. Herodotou, M. Totomis, N. Bennett, Biofouling resistance of titanium dioxide and zinc oxide nanoparticulate silane/siloxane exterior facade treatments, Build. Environ. 59 (2013) 47–55.

[26] L. Graziani, E. Quagliarini, A. Osimani, L. Aquilanti, F. Clementi, M. D'Orazio, The influence of clay brick substratum on the inhibitory efficiency of TiO2 nanocoating against biofouling, Build. Environ. 82 (2014) 128–134. http://linkinghub.elsevier.com/retrieve/pii/S0360132314002650 (accessed September 3, 2014).

[27] L. Graziani, E. Quagliarini, A. Osimani, L. Aquilanti, F. Clementi, C. Yéprémian, V. Lariccia, S. Amoroso, M. D'Orazio, Evaluation of inhibitory effect of TiO2 nanocoatings against microalgal growth on clay brick façades under weak UV exposure conditions, Build. Environ. 64 (2013) 38–45.

[28] J. Radulovic, J. MacMullen, Z. Zhang, H.N. Dhakal, S. Hannant, L. Daniels, J. Elford, C. Herodotou, M. Totomis, N. Bennett, Biofouling resistance and practical constraints of titanium dioxide nanoparticulate silane/siloxane exterior facade treatments, Build. Environ. 68 (2013) 150–158. http://linkinghub.elsevier.com/retrieve/pii/S0360132313001923 (accessed November 26, 2013).

[29] J.G. Castaño, E. Velilla, L. Correa, M. Gómez, F. Echeverría, Ceramic insulators coated with titanium dioxide films: Properties and self-cleaning performance, Electr. Power Syst. Res. 116 (2014) 182–186. http://linkinghub.elsevier.com/retrieve/pii/S0378779614002181 (accessed July 9, 2014).

[30] E. Franzoni, A. Fregni, R. Gabrielli, G. Graziani, E. Sassoni, Compatibility of photocatalytic TiO2-based finishing for renders in architectural restoration : A preliminary study, Build. Environ. 80 (2014) 125–135.

[31] P. Munafò, G.B. Goffredo, E. Quagliarini, TiO2-based nanocoatings for preserving architectural stone surfaces: An overview, Constr. Build. Mater. 84 (2015) 201–218. doi:10.1016/j.conbuildmat.2015.02.083.

[32] M. Aflori, B. Simionescu, I.-E. Bordianu, L. Sacarescu, C.-D. Varganici, F. Doroftei, A. Nicolescu, M. Olaru, Silsesquioxane-based hybrid nanocomposites with methacrylate units containing titania and/or silver nanoparticles as antibacterial/antifungal coatings for monumental stones, Mater. Sci. Eng. B. 178 (2013) 1339–1346.

[33] C. Kapridaki, P. Maravelaki-Kalaitzaki, TiO2–SiO2–PDMS nano-composite hydrophobic coating with self-cleaning properties for marble protection, Prog. Org. Coatings. 76 (2013) 400–410. http://www.sciencedirect.com/science/article/pii/S0300944012002676.

[34] S. a Ruffolo, A. Macchia, M.F. La Russa, L. Mazza, C. Urzì, F. De Leo, M. Barberio, G.M. Crisci, Marine Antifouling for Underwater Archaeological Sites : TiO 2 and Ag-Doped TiO 2, Int. J. Photoenergy. 2013 (2013).

[35] M. D'Orazio, G. Cursio, L. Graziani, L. Aquilanti, A. Osimani, F. Clementi, C. Yéprémian, V. Lariccia, S. Amoroso, Effects of water absorption and surface roughness on the bioreceptivity of ETICS compared to clay bricks, Build. Environ. 77 (2014) 20–28. http://linkinghub.elsevier.com/retrieve/pii/S036013231400078X (accessed April 15, 2014).

[36] T. Martinez, A. Bertron, G. Escadeillas, E. Ringot, Algal growth inhibition on cement mortar : Efficiency of water repellent and photocatalytic treatments under UV/VIS illumination, Int. Biodeterior. Biodegradation. 89 (2014) 115–125. http://dx.doi.org/10.1016/j.ibiod.2014.01.018.

[37] H. Barberousse, R.J. Lombardo, G. Tell, A. Coute, Factors involved in the colonisation of building facades by algae and cyanobacteria in France, Biofouling. 22 (2006) 69–77. <Go to ISI>://000237646400001.

[38] J.J. Ortega-Calvo, X. Ariño, M. Hernandez-Marine, C. Saiz-Jimenez, Factors affecting the weathering and colonization of monuments by phototrophic microorganisms, Sci. Total Environ. 167 (1995) 329–341. http://www.sciencedirect.com/science/article/pii/004896979504593P.

[39] A. Dubosc, G. Escadeillas, P.J. Blanc, Characterization of biological stains on external concrete walls and influence of concrete as underlying material, Cem. Concr. Res. 31 (2001) 1613–1617. http://www.sciencedirect.com/science/article/pii/S0008884601006135.

[40] T.H. Tran, A. Govin, R. Guyonnet, P. Grosseau, C. Lors, E. Garcia-Diaz, D. Damidot, O. Devès, B. Ruot, Influence of the intrinsic characteristics of mortars on biofouling by Klebsormidium flaccidum, Int. Biodeterior. Biodegradation. 70 (2012) 31–39.

[41] F. Wang, G. Sun, W. Zhang, L. Yang, P. Liu, Performance of photocatalytic cementitious material: Influence of substrate surface microstructure, Constr. Build. Mater. 110 (2016) 175–181. doi:10.1016/j.conbuildmat.2015.11.030.

[42] E. Kowalska, Z. Wei, B. Karabiyik, A. Herissan, M. Janczarek, M. Endo, A. Markowska-Szczupak, H. Remita, B. Ohtani, Silver-modified titania with enhanced photocatalytic and antimicrobial properties under UV and visible light irradiation, Catal. Today. 252 (2015) 136–142. http://linkinghub.elsevier.com/retrieve/pii/S0920586114007263 (accessed June 23, 2015).

[43] K. Naik, M. Kowshik, Anti-biofilm efficacy of low temperature processed AgCl-TiO2 nanocomposite coating., Mater. Sci. Eng. C. Mater. Biol. Appl. 34 (2014) 62–8. http://www.ncbi.nlm.nih.gov/pubmed/24268234 (accessed June 23, 2015).

[44] J. MacMullen, Z. Zhang, H.N. Dhakal, J. Radulovic, A. Karabela, G. Tozzi, S. Hannant, M.A. Alshehri, V. Buhé, C. Herodotou, M. Totomis, N. Bennett, Silver nanoparticulate enhanced aqueous silane/siloxane exterior facade emulsions and their efficacy against algae and cyanobacteria biofouling, Int. Biodeterior. Biodegradation. 93 (2014) 54–62. http://linkinghub.elsevier.com/retrieve/pii/S0964830514001449 (accessed October 14, 2014).

[45] D. Pinna, B. Salvadori, M. Galeotti, Monitoring the performance of innovative and traditional biocides mixed with consolidants and water-repellents for the prevention of biological growth on stone., Sci. Total Environ. 423 (2012) 132–41. http://www.ncbi.nlm.nih.gov/pubmed/22401787 (accessed June 23, 2015).

[46] UNI EN 623-4:1994. Advanced technical ceramics - Monolithic ceramics - General and textural properties - Part 4: Determination of surface roughness., Ente nazionale italiano di unificazione, 2005.

[47] UNI EN ISO 4287:2009 - Geometrical Product Specifications (GPS) - Surface texture: Profile method - Terms, definitions and surface texture parameters., International Standards Organization, 2009.

[48] ASTM D4404 - 10. Standard Test Method for Determination of Pore Volume and Pore Volume Distribution of Soil and Rock by Mercury Intrusion Porosimetry., American Society for Testing and Materials, 2010.

[49] UNI EN 15886:2010 Conservation of cultural property - Test methods - Colour measurement of surfaces, Ente nazionale italiano di unificazione, 2010.

[50] L. Graziani, E. Quagliarini, F. Bondioli, M. D'Orazio, Durability of self-cleaning TiO2 coatings on fired clay brick façades: Effects of UV exposure and wet & dry cycles, Build. Environ. 71 (2014) 193–203.

[51] UNI, UNI 11259:2008, Determ. Photocatalytic Act. Hydraul. Bind. - Rodammina Test Method. (2008) 10.

[52] S. Scheerer, O. Ortega- Morales, C. Gaylarde, Chapter 5 - Microbial Deterioration of Stone Monuments—An Updated Overview, Adv. Appl. Microbiol. 66 (2009) 97–139. http://www.sciencedirect.com/science/article/pii/S0065216408008058.

[53] T.H. Tran, A. Govin, R. Guyonnet, P. Grosseau, C. Lors, D. Damidot, O. Devès, B. Ruot, Avrami's law based kinetic modeling of colonization of mortar surface by alga Klebsormidium flaccidum, Int. Biodeterior. Biodegradation. 79 (2013) 73–80. http://linkinghub.elsevier.com/retrieve/pii/S0964830512003344 (accessed October 29, 2013).

[54] L. Graziani, E. Quagliarini, M. D'Orazio, TiO2 -treated different fired brick surfaces for biofouling prevention: Experimental and modelling results, Ceram. Int. 42 (2016) 4002–4010.

[55] G. Sharma, C.R.C. Press, Digital color imaging handbook, CRC Press, U.S.A., 2002.

[56] E. Quagliarini, F. Bondioli, G.B. Goffredo, A. Licciulli, P. Munafò, Smart surfaces for architectural heritage: Preliminary results about the application of TiO2-based coatings on travertine, J. Cult. Herit. 13 (2012) 204–209.

[57] G.D. Davies, Biofilm Dispersion, in: H.-C. Flemming, J. Wingender, U. Szewzyk (Eds.), Biofilm Highlights, Springer Berlin Heidelberg, Berlin, Heidelberg, 2011. http://link.springer.com/10.1007/978-3-642-19940-0 (accessed March 26, 2015).

## Figure captions



## Table captions

**Table 1**
Click here to download Table: Table 1.docx

**Table 1** Intrinsic characteristics of tested clay brick specimens (mean value ± standard deviation). Each sample is representative of three specimens.

| Sample | Treatment | Total porosity (%) | Ra (µm) | Rz (µm) | Rmax (µm) |
|---|---|---|---|---|---|
| ANt | Untreated | | | | |
| AAg | $T_iO_2$ - Ag | 36.65 ± 0.65 | 8.90 ± 0.90 | 57.00 ± 8.00 | 68.00 ± 14.00 |
| ACu | $T_iO_2$ - Cu | | | | |
| NNt | Untreated | | | | |
| NAg | $T_iO_2$ – Ag | 19.13 ± 1.66 | 2.80 ± 0.50 | 27.00 ± 4.00 | 39.00 ± 6.00 |
| NCu | $T_iO_2$ – Cu | | | | |

**Table 2** Average color variation after coating application expressed as CIELab color coordinates and total color differences (ΔE).

| Sample | ΔL* | Δa* | Δb* | ΔE |
|---|---|---|---|---|
| ANt | --- | --- | --- | --- |
| AAg | 6.22 | -1.51 | -2.05 | 6.73 |
| ACu | 6.36 | -1.74 | -2.71 | 7.13 |
| NNt | --- | --- | --- | --- |
| NAg | 3.13 | -3.52 | -6.88 | 8.34 |
| NCu | 2.23 | -2.98 | -6.21 | 7.24 |

**Table 3**
Click here to download Table: Table 3.docx

**Table 3** Calculated parameters of N group (Avrami model)

| Sample | $t_1$ (day) | $k_g$ (x $10^{-10}$) (Spot/µm$^2$ day$^2$) | $k_c$ *(exp)* (µm/day) | $K$ (x $10^{-6}$) (Spot/day$^4$) | R (%) | $k_c$ *(calc)* (µm/day) |
|---|---|---|---|---|---|---|
| NNt | 21 | 568.52 | 45.91 | 0.23 | 26.28 | 23.11 |
| NAg | 28 | 1512.4 | 27.74 | 1.41 | 27.21 | 10.80 |
| NCu | 35 | 904.65 | 32.66 | 0.86 | 16.66 | 13.19 |

**Table 4**
Click here to download Table: Table 4.docx

**Table 4** Calculated parameters of A group (4PL model)

| Sample | $t_1$ (day) | *A (%)* | *B (%)* | *C (days)* | D |
|---|---|---|---|---|---|
| ANt | 0 | 0 | 89.21 | 7 | 2.02 |
| AAg | 0 | 0 | 90.41 | 7 | 1.49 |
| ACu | 0 | 0 | 94.91 | 7 | 1.59 |

Figure 1

Click here to download high resolution image

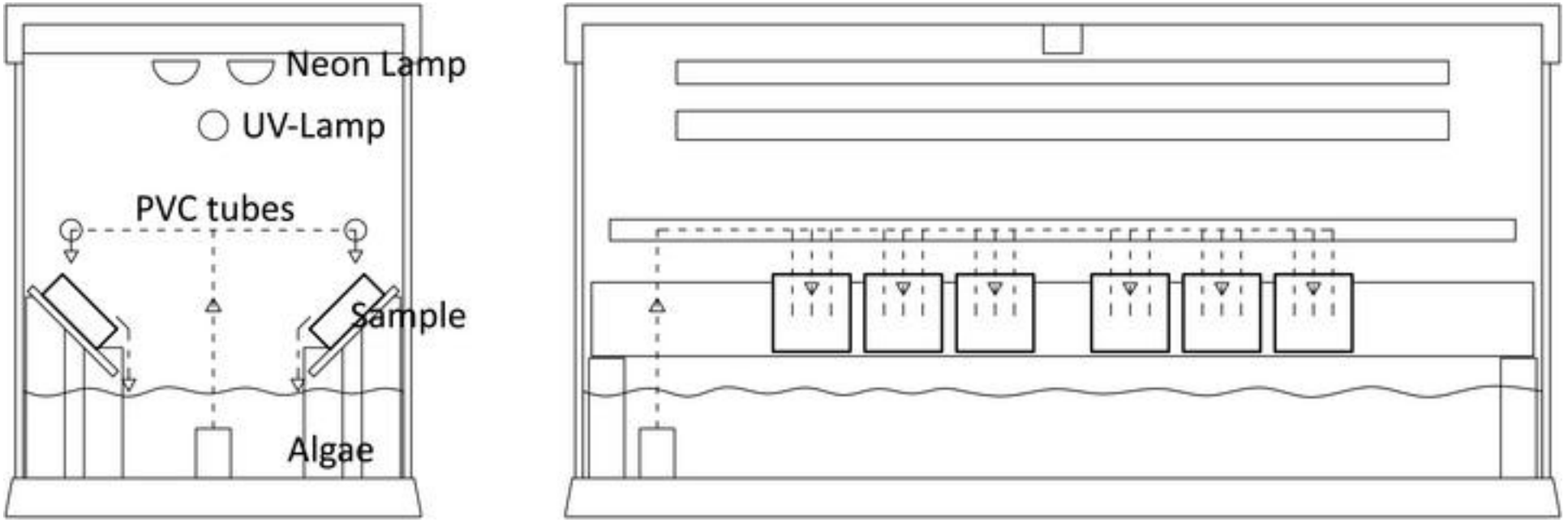

Figure 2

Click here to download high resolution image

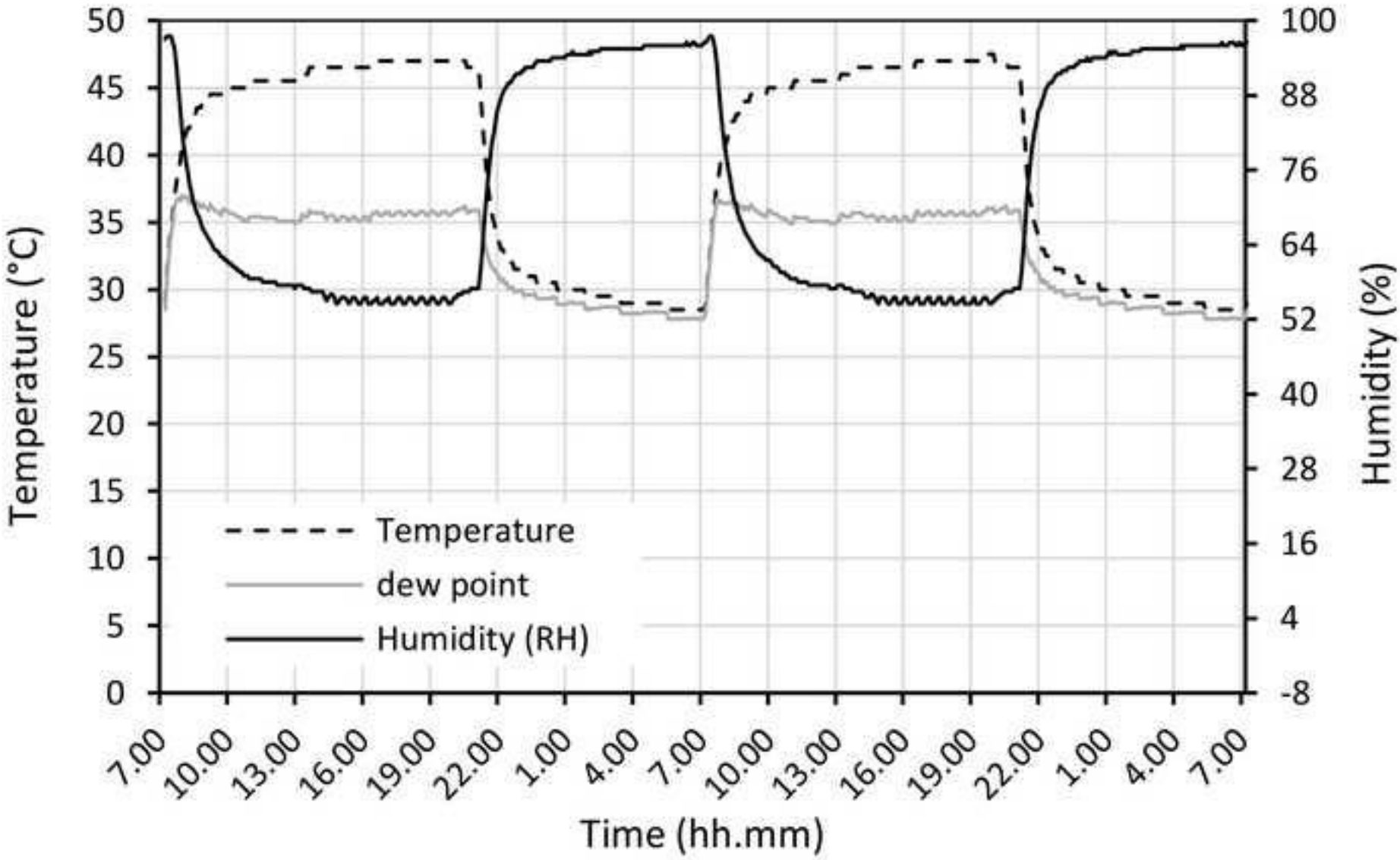

Figure 3

Click here to download high resolution image

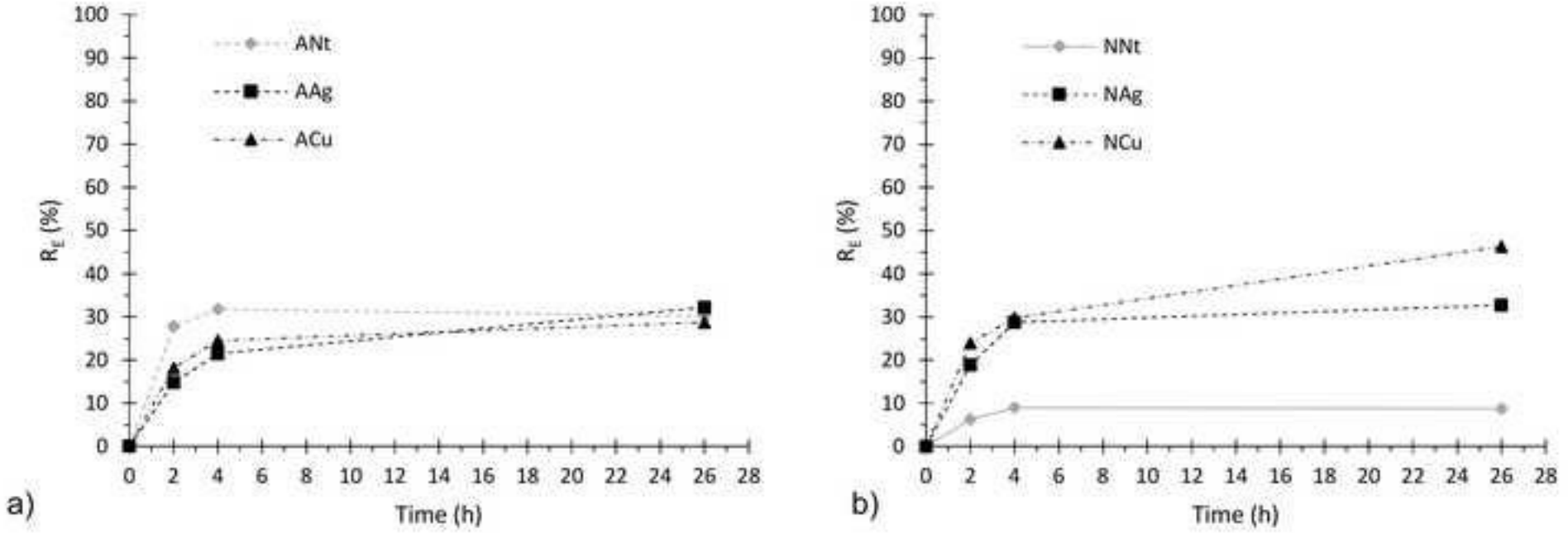

Figure 4

Click here to download high resolution image

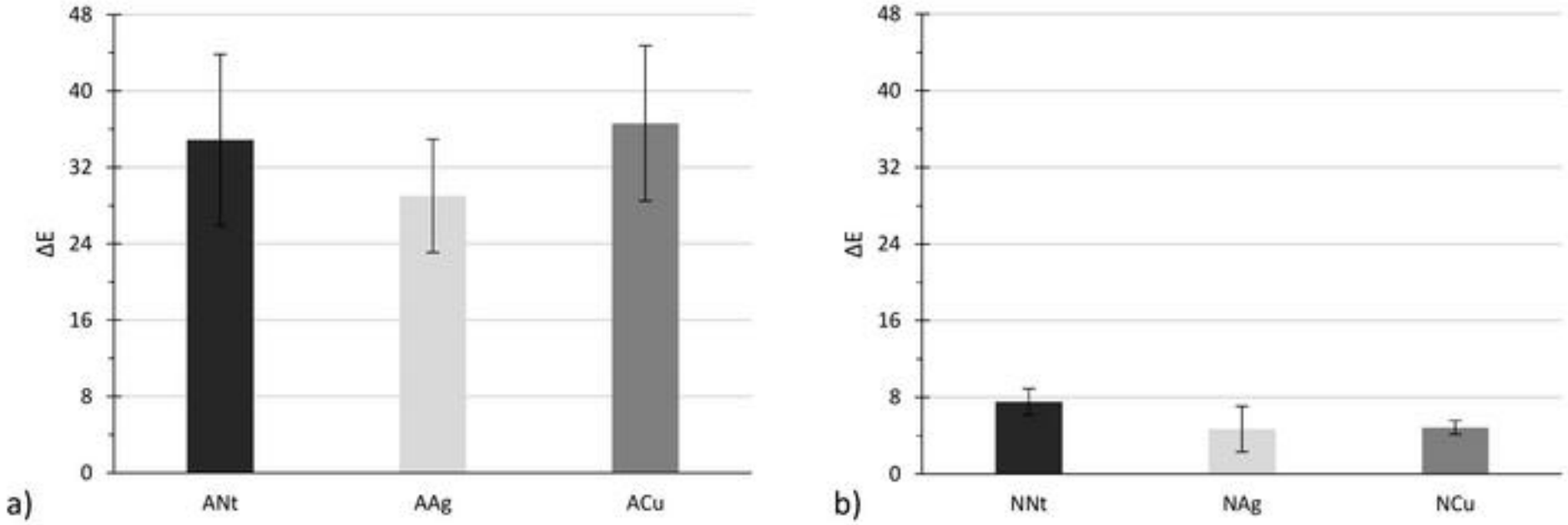

Figure 5
Click here to download high resolution image

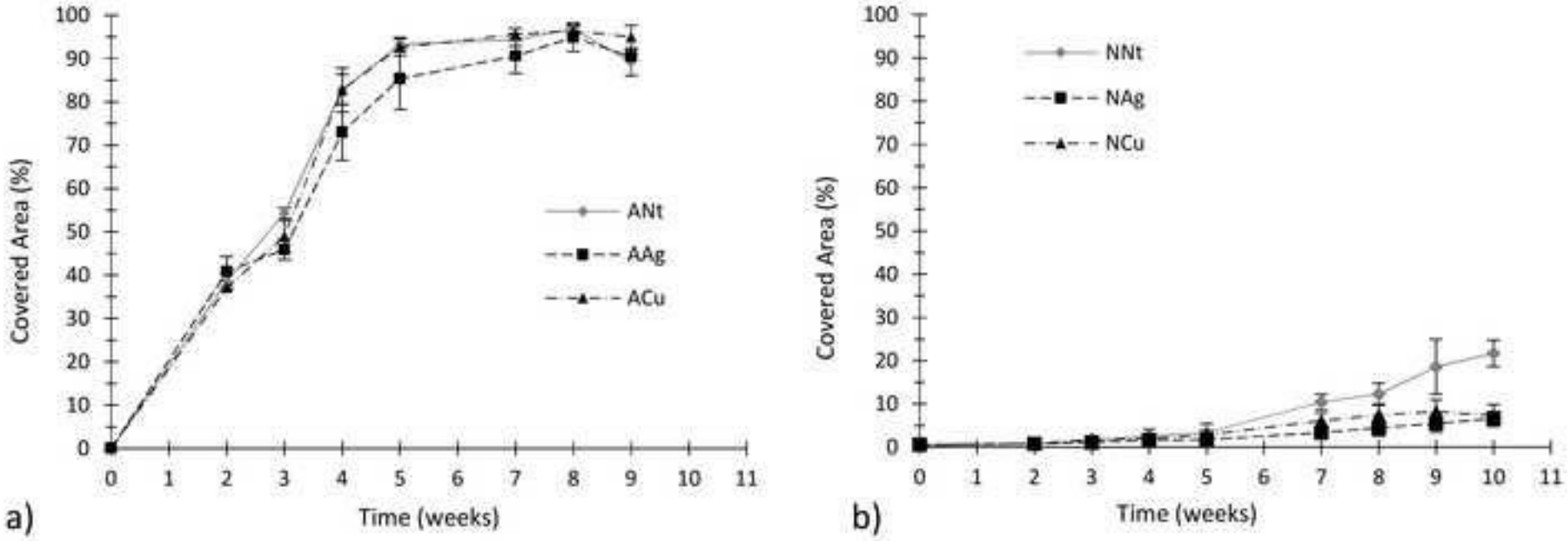

Figure 6
Click here to download high resolution image

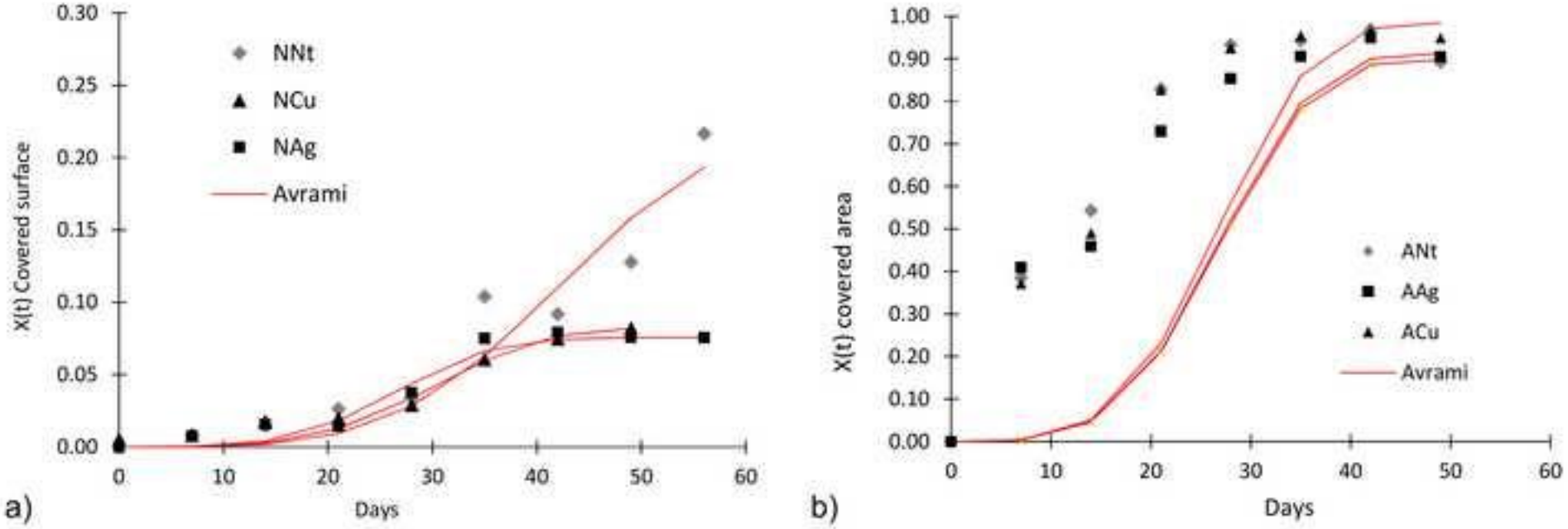

Figure 7

Click here to download high resolution image